



Efficient heavy metals and salts rejection using a novel modified polysulfone nanofiltration membrane

F. Gholami¹ · A. Asadi² · A. A. Zinatizadeh^{1,3}

Received: 21 January 2022 / Accepted: 4 April 2022 / Published online: 6 May 2022
© The Author(s) 2022

Abstract

Recent research proclivity is about supplying water for drinking, urban and industrial applications which is recognized as one of the most significant challenges that threaten humanity. Giving its simplicity and high efficient yield, membrane technology has been preferred compared to other separation technologies for water and wastewater treatment. In the present research, KIT-6 (KIT: Korea Advanced Institute of Science and Technology) was functionalized by H-acid to improve hydrophilic functional groups on KIT-6 surface. Different characterization tests were performed to prove the insertion of H-acid on KIT-6 (H-KIT-6), e.g., FT-IR, XRD, zeta potential and FESEM analysis. Also, the effects of different loading of KIT-6 and H-KIT-6 on the morphology, characteristics and performance of Polysulfone (PSf) nanofiltration (NF) membranes were investigated. The maximum pure water flux (30.2 kg/m² h), the lowest irreversible fouling ratio (3.96%) and the highest flux recovery ratio (96.04%) were obtained for the membrane embedded with 0.1 wt.% H-KIT-6 (optimum membrane). Also, the performance of the synthesized membranes was evaluated by rejection of four different salts (K₂SO₄, MgSO₄, KCl and NaCl) and heavy metal ions (As³⁺ and Hg²⁺). The NF membrane embedded with 0.1 wt.% H-KIT-6 also presented the highest rejection of different salts and heavy metal ions (As³⁺ = 99.85% and Hg²⁺ = 99.27%) compared to the others. Finally, the performance of the optimum membrane to treat a real case of Gachsaran brackish water was assessed. As a result, by applying the optimum membrane, 565 mg/l, 28 mg/l and 27 mg/l of Ca²⁺, SO₄²⁻ and Mg²⁺ were rejected, respectively.

Keywords Heavy metals · Nanofiltration · H-KIT-6 · Gachsaran brackish water

Introduction

Water shortage has been considering as a foremost problem in all over the world over the years. Application of cost effective and high efficiency technologies to treat wastewaters and brackish water could be a decent solution to solve this concern. Numerous biological, physical and chemical methods and also couple of them were applied to treat different wastewaters. Besides, salts could be separated from brackish water via evaporation, ion exchange and membrane technology to obtain drinking water (Giagnorio et al.

2018; Zhao et al. 2020). Among the mentioned processes, membrane technology has been recognized as a promising technology due to its appropriate features such as its simple operation, high rejection of solutes and being cost effective (Kiran et al. 2016; López et al. 2020).

Two main processes in membrane technology which could be applied to treat salty water are reverse osmosis (RO) and nanofiltration (NF). Also, it should be mentioned that the presence of heavy metals in water resources is a treat to human health which could be removed along with other ions by RO and NF processes (Ikehata et al. 2018; Wang et al. 2020). As reported in the literature, heavy metals could aggregate in the cells of different organs in human body and abolish the cellular functions with making changes in proteins and nucleic acids, resulting several diseases in some vital organs like the lungs, liver, kidneys and even the central nervous function. Long-term arsenic poisoning via contaminated drinking water caused skin diseases like lesion, swollen skin and cancer (Podgorski & Berg, 2020; Zeng et al. 2020). Mercury also is known as a dangerous

✉ A. Asadi
Azarasadi_88@yahoo.com; a.asadi@yu.ac.ir

¹ Department of Applied Chemistry, Faculty of Chemistry, Razi University, Kermanshah P.O. Box 67144-14971, Iran

² Department of Gas and Petroleum, Yasouj University, Gachsaran 75918-74831, Iran

³ Department of Environmental Sciences, University of South Africa, Pretoria, South Africa

heavy metal which creates different symptoms in human body like hearing, speaking and seeing damages, muscle weakness, nervousness and memory loss. Its long-term complications are kidney damage and a reduction in brainpower (Sutton et al. 2002).

RO is an impressive technique to purify polluted and brackish water; however, it is required high operating pressure and also its fouling is drastic (Wang et al. 2018). Because of the mentioned cons for RO process, NF process is being considered as an efficient replacement for RO process to separate multivalent ions and heavy metals from water resources. NF technology is operated in lower operating pressure that resulted in lower fouling phenomena rather than RO process which these features make it efficient technology in terms of energy consumption and economic aspects (Chitpong & Husson, 2017; Gao et al. 2020; Moradi et al. 2021).

Different NF membranes were synthesized by various polymers like polyvinylidene fluoride (PVDF) (Abbasi Eskandary et al. 2021), polyacrylonitrile (PAN) (Li et al. 2021), polyether sulfone (PES) (Gholami et al. 2021), polyether imide (PEI) (Zhao et al. 2021), polysulfone (PSf) (Li et al. 2022) and so on. Each of the mentioned polymer has some pros and cons. PS is a high-performance thermoplastic with high toughness and stability at high temperatures which could be considered as an appropriate case to synthesize membranes. The restriction of using PSf polymers as a matrix membrane is its low resistance for clogging and fouling phenomena. Application of hydrophilic additives into matrix membranes improved hydrophilicity, surface smoothness and rejection rate and also led to lower fouling phenomena and nearly stable permeate flux (Rahimi et al. 2021). In this regard, various hydrophilic additives have been incorporated into polymer matrix for instance, $\text{Fe}_3\text{O}_4/\text{SiO}_2\text{-NH}_2$ nanocomposite (Kamari & Shahbazi, 2020), curcumin-modified boehmite nanoparticles (Moradi et al. 2020), rGO/ZnO (Li et al. 2022), mesoporous (Asadi et al. 2022a, b) and metal-organic framework (MOF) (Gnanasekaran et al. 2021).

Mesoporous silica and carbon materials are used intensively as fillers in mixed matrix membrane due to their high specific surface area and hydrothermal resistance (Samari et al. 2021). In this regard, KIT-6 was introduced as a mesoporous filler to tailor NF membrane to remove salt/dye/heavy metal from water in NF composite membrane by Moradi and her coworkers. From the reported results, heavy metals such as Mn^{2+} , Cu^{2+} , Ni^{2+} and Pb^{2+} , as well as a salt solution of Na_2SO_4 , which reported a reduction of over 90% (Moradi et al. 2021).

In the present research, KIT-6 was considered as a main filler in PSF via its large average pore diameter (4–12 nm), wall thickness of 4 to 6 nm and a tridimensional symmetric cubic structure which could improve water flux of the PSF

membrane. Moreover, KIT-6 was functionalized with H-acid to improve its hydrophilic properties. H-acid is a naphthalene with two $-\text{SO}_3\text{H}$, $-\text{NH}_2$ and $-\text{OH}$ bonds on its surface. Therefore, it is expected that the membrane embedded with KIT-6 presents more hydrophilic and antifouling properties along with enhanced pure water flux.

In order to clarify the effect of H-acid on the properties of KIT-6, FTIR spectrum, XRD pattern, FESEM image and zeta potential test for H-KIT-6 and KIT-6 were performed. Moreover, in order to portray the effects of KIT and KIT-6 as fillers on the properties and performance of the membranes, two series NF membranes with PSf as a matrix polymer and different loading of H-KIT-6 and KIT-6 were synthesized through the phase inversion method. It's worth mentioning that KIT-6 functionalized with H-acid was not reported already in the literature and aiming to shed light on the effects of two different fillers on the membrane performance, the rejection of four different salts (K_2SO_4 , MgSO_4 , KCl and NaCl) and two heavy metal ions (Hg^{2+} and As^{3+}) were evaluated. Finally, the obtained optimum membrane was applied for treating a real case of brackish water given from Gachsaran city located in Iran. As a notice, drinking water of Gachsaran city was supplied by some wells which is well known as salty water containing high values of different salts and it is required to be treated before using.

Experiments

Materials

Methanol anhydrous (CH_3OH , 99.8%), polyethylene glycol (PEG) at different molecular weights, acetone, chloroacetic acid, sodium chloride, potassium chloride, potassium sulfate, magnesium sulfate and poly(ethylene glycol)-block-poly(propylene glycol)-block-poly(ethylene glycol) (P123, $\text{Mn} = 5800$, $(\text{EO})_{20}(\text{PO})_{70}(\text{EO})_{20}$) were purchased from Sigma-Aldrich. Mercury(II) sulfate (Hg^{2+}), arsenite (As^{3+}), ethanol ($\geq 99.9\%$), tetraethoxysilane (TEOS, 98%), *n*-butanol, polyvinylpyrrolidone (PVP, $\text{Mw} = 25,000$ g/mol), thionyl chloride (97%), *N,N*-dimethylacetamide (DMAc, $\geq 99.0\%$) and hydrochloric acid (HCl, 37%) were provided from Merck Co. Polysulfone (PSf) was provided from BASF Co. (Germany).

KIT-6 modification

KIT-6 was prepared based on the procedure reported in the literature (Wang et al. 2015). After that, H-acid-functionalized KIT-6 (H-KIT-6) mesoporous was provided. In this regard, 1 g of the chloro-modified KIT-6 mesoporous and 1 g of H-acid was thoroughly dissolved in toluene and

refluxed overnight. Finally, the solution was dried at 100 °C to yield the H-KIT-6 mesoporous (Samari et al. 2021).

Fabrication of mixed matrix membranes

Phase inversion method was applied to synthesize mixed matrix membranes. Different casting solutions were prepared according to Table 1. Different weight percent of powdered KIT-6 and H-KIT-6 (0, 0.1, 0.5 and 1.0 wt.%) were distributed in DMAc via sonication (45 min) followed by stirring (1 h) to get uniform casting solution and to avoid occurring agglomeration. Then, PSf (20 wt.%) and PVP (1 wt.%) were added to the solution and stirred overnight to achieve homogenous viscous solution. In the next step, the casting solution was poured on a flat glass plate using an applicator. The casted plate was immersed immediately in deionized water coagulation bath. The fabricated membrane was detached from the glass plate within a few minutes. After detaching the obtained film, the membrane was kept in deionized water overnight (Gholami et al. 2021).

Dead-end setup and fouling/rejection tests

To evaluate the performance of the fabricated membranes in terms of pure water flux, antifouling properties, and rejection of different salts and heavy metal ions, a dead-end setup with a membrane surface area of 0.001256 m² was utilized. To provide the required pressure (4 bar) to operate the dead-end setup, nitrogen gas was used. At first, distilled water was passed through the dead-end setup and pure water flux was calculated based on the following equation:

$$J_0 = \frac{M}{A_m \cdot \Delta t} \tag{1}$$

In the next step, to evaluate fouling phenomenon, dried milk powder with concentration of 1000 mg/l was used as a foulant agent. In this mean, firstly distilled water was passed through to obtain pure water flux (J_0), then dried milk solution was filtered for 90 min (J_p), afterward the

membrane was washed and immersed into distilled water (20 min), and finally, the distilled water was filtered again for 60 min (J_R) (Samari et al. 2020).

The flux recovery ratio (FRR), irreversible, reversible and total fouling resistances were calculated using the below equations:

$$FRR(\%) = \left(\frac{J_R}{J_0} \right) \times 100 \tag{2}$$

$$R_{ir} = \left(\frac{J_0 - J_R}{J_0} \right) \times 100 \tag{3}$$

$$R_r = \left(\frac{J_R - J_p}{J_0} \right) \times 100 \tag{4}$$

$$R_t = \left(1 - \frac{J_p}{J_0} \right) \tag{5}$$

where R_{ir} , R_r and R_t refer to the irreversible, reversible and total fouling resistances, respectively.

Also, the rejection of different salts and heavy metals was evaluated based on Eq. 6.

$$R(\%) = (1 - C_p/C_f) \times 100 \tag{6}$$

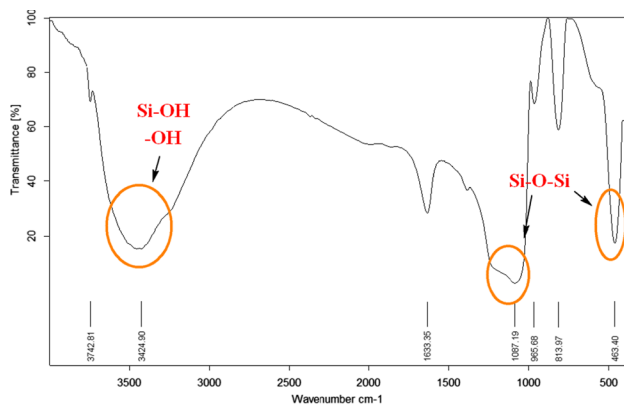
where M , A_m and Δt refer to the weight of collected permeate in kg, effective area of membrane in m² and test time in h. C_p and C_f signify the concentration of studied pollutants after (in permeate stream) and before (in feed stream) filtration, respectively. The concentration of salts and heavy metal ions (Hg^{2+} and As^{3+}) in each solution was measured using a conductive meter and atomic absorption spectroscopy (AAS), respectively. It should be mentioned that mercury(II) sulfate (Hg^{2+}) and arsenite (As^{3+}) with concentration of 10, 20 and 50 mg/l were prepared in deionized water for heavy

Table 1 The casting solution composition for membrane preparation

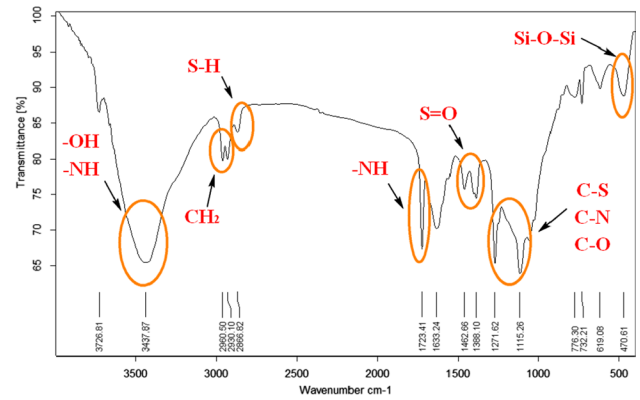
Membrane type	PES (wt.%)	PVP (wt.%)	DMAc (wt.%)	Additive (wt.%)
M1	20	1	79	–
M2	20	1	78.9	0.1 ^a
M3	20	1	78.5	0.5 ^a
M4	20	1	78	1.0 ^a
M5	20	1	78.9	0.1 ^b
M6	20	1	78.5	0.5 ^b
M7	20	1	78	1.0 ^b

^aKIT-6

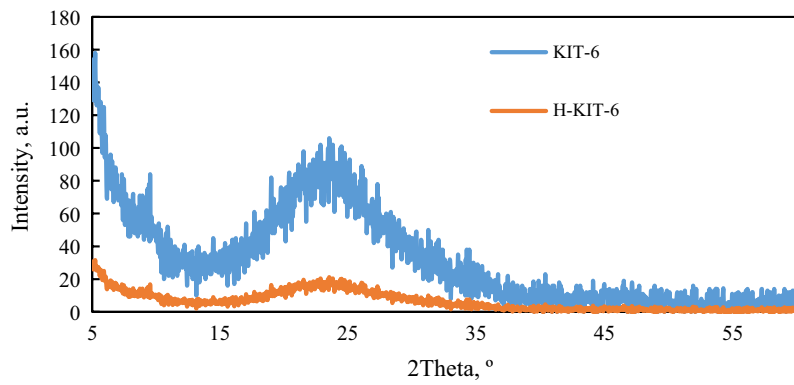
^bH-KIT-6



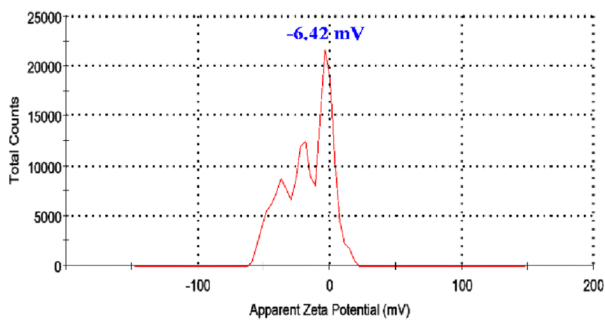
(a)



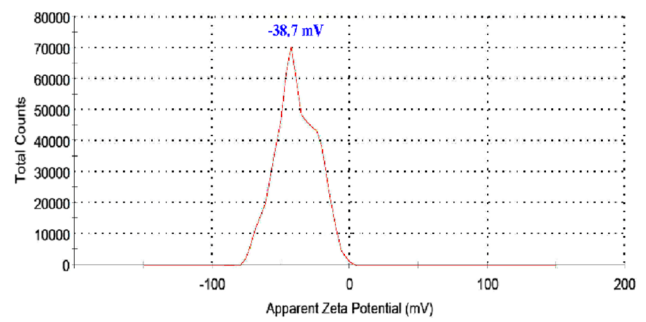
(b)



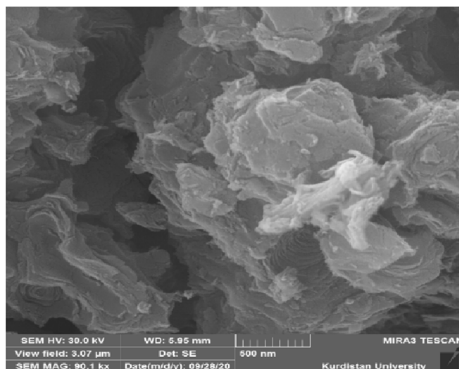
(c)



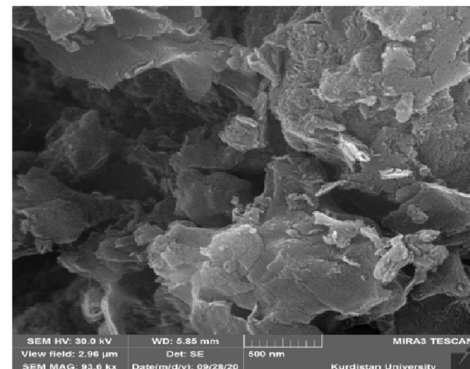
(d)



(f)



(e)



(h)

◀**Fig. 1** FT-IR spectrum of KIT-6 (**a**) and H-KIT-6 (**b**), wide-angle XRD pattern for both KIT-6 and H-KIT-6 (**c**), zeta potential of KIT-6 (**d**) and H-KIT-6 (**f**), FESEM image of KIT-6 (**e**) and H-KIT-6 (**h**)

metals and 0.2 g/L of different salts (K_2SO_4 , $MgSO_4$, KCl and NaCl) was dissolved in deionized water.

In addition, to investigate the multipollutant separation of the membranes, a real case of brackish water obtained from Gachsaran city located in Iran was passed through

the optimum membrane. The concentrations of SO_4^{2-} , Ca^{2+} and Mg^{2+} and total hardness of Gachsaran brackish water were measured before and after filtration according to standard methods.

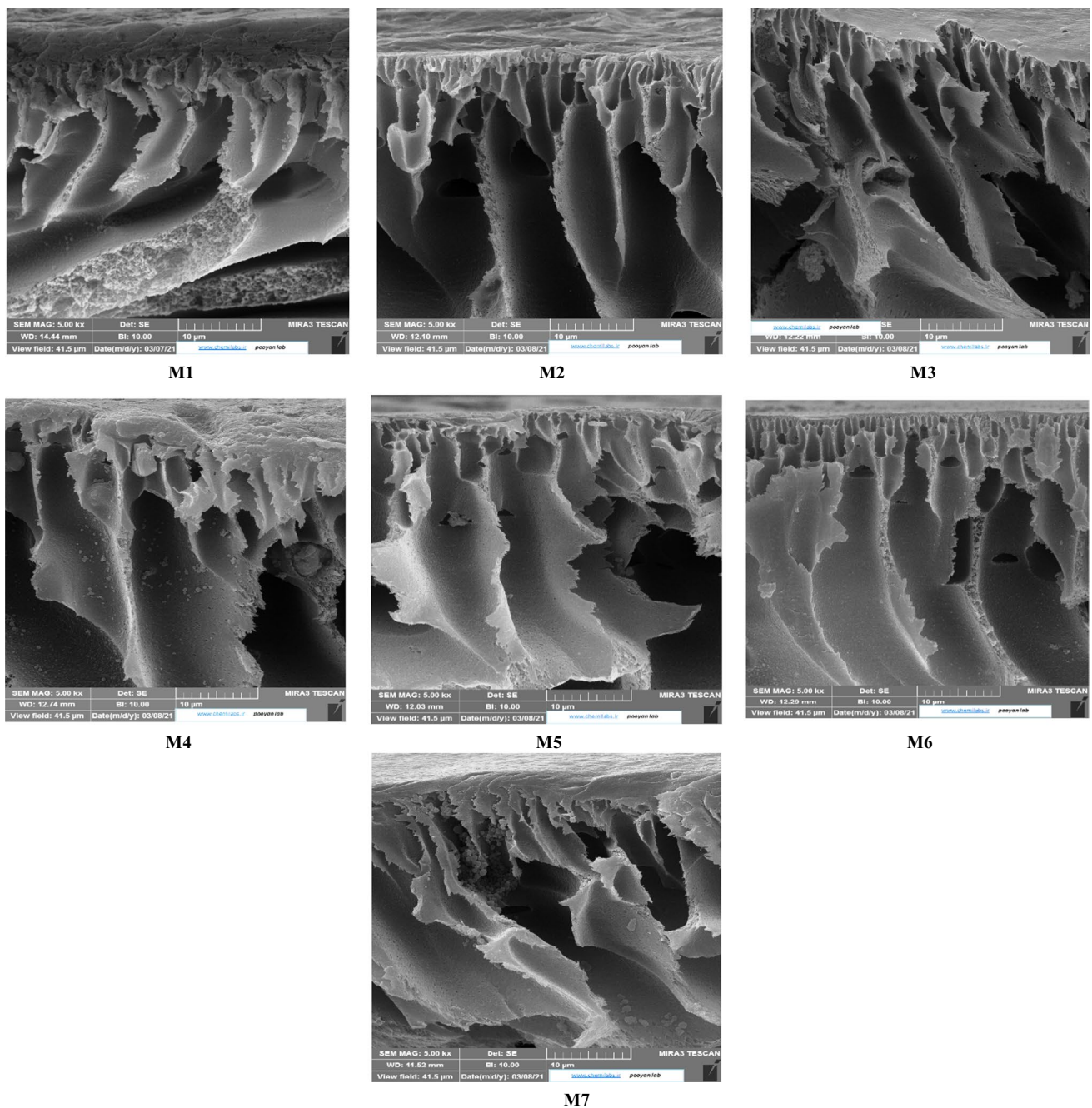


Fig. 2 FESEM images of the fabricated membranes

Characterization of fabricated membranes

In order to investigate the characterization of KIT-6 and H-KIT-6 and also fabricated membranes embedded with the additives, some characterization tests like field emission scanning electron microscope (FESEM), Fourier transform infrared (FT-IR), X-ray diffraction analysis,

zeta potential, atomic force microscopy (AFM) and water contact angle were applied.

The morphology of synthesized H-KIT-6 mesoporous and cross-sectional morphology of the fabricated membranes was evaluated by FESEM (TESCAN, MIRA III, Czech). The chemical structure of KIT-6 and H-KIT-6 mesoporous was assessed using FT-IR (Nicolet Avatar 370). Also, the material chemical features of the synthesized mesoporous were tested by XRD

Table 2 Water contact angle, porosity, μ_p and MWCO of the fabricated membrane

Membrane samples	Water contact angle (degree)	Porosity (%)	μ_p (nm)	MWCO (Da)
M1	66.6 ± 2.0	69.6 ± 2.1	1.61	1057
M2	53.4 ± 2.1	74.2 ± 2.1	1.37	785
M3	46.2 ± 2.2	81.0 ± 2.2	1.19	610
M4	51.2 ± 2.1	69.3 ± 2.2	1.27	685
M5	37.9 ± 0.56	84.7 ± 1.3	0.70	240
M6	42.1 ± 0.63	79.8 ± 1.2	0.72	250
M7	45.5 ± 0.68	63.8 ± 0.9	0.78	284

(Philips PW 1730, Holland). To determine surface charge of H-KIT-6 mixed matrix NF membranes, zeta potential as a function of pH from 4 to 10 was measured by a SurPASS electrokinetic analyzer (Graz, Austria). Besides, the surface topology was carried out by a nanosurf Mobile-S AFM. The water contact angle of the fabricated membranes was measured by using a contact angle goniometer Dataphysics OCA15 plus μ , Filderstadt.

The weights of the dry and wet membranes were measured to calculate the overall porosity of the membranes using the following equation at the temperature of 25 °C:

$$\varepsilon(\%) = (m_{wet} - m_{dry}) / (\rho \cdot A_m \cdot L) \times 100 \tag{7}$$

where m_{wet} and m_{dry} denote the weights of the wet (with deionized water) and dry membrane in kg, respectively. ρ , A_m , and L are the density of water (kg/m³), the effective area of membrane (m²) and the membrane thickness (m), respectively.

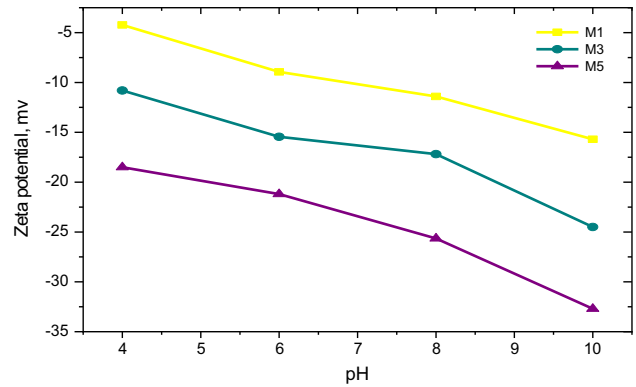


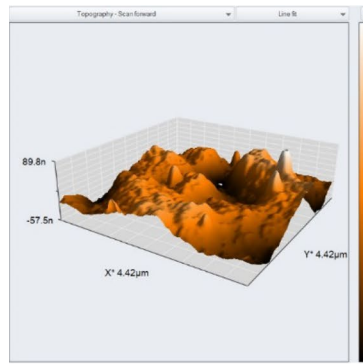
Fig. 3 Zeta potential of the M1, M3 and M5 at different pH

Besides, mean pore radius (r_m) was calculated according to Guerout–Elford–Ferry Eq. (8):

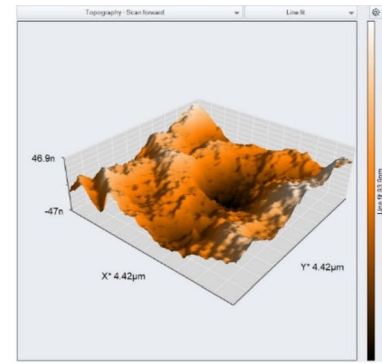
$$r_m = \sqrt{\frac{(2.9 - 1.75\varepsilon) \times 8\eta|Q}{\varepsilon \times A \times \Delta P}} \tag{8}$$

where η is the water viscosity (8.9×10^{-4} Pa s), Q is the volume of the permeate pure water per unit time (m³/s) and ΔP is the operating pressure (0.5 M Pa) (Moradi et al. 2020).

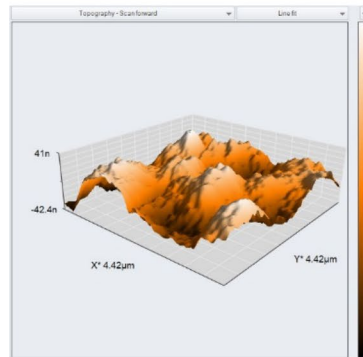
Fig. 4 AFM images of the prepared membranes



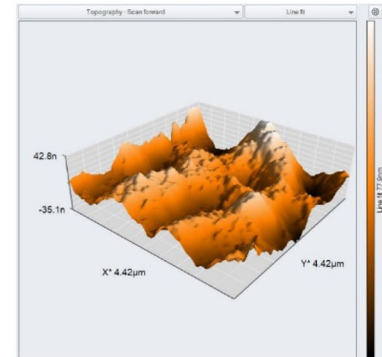
M1



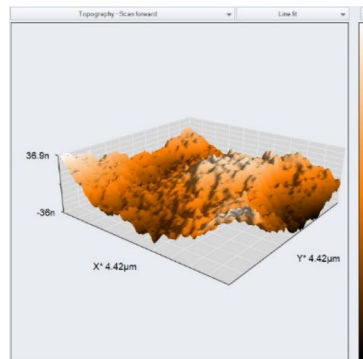
M2



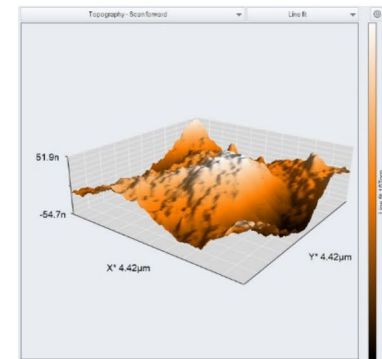
M3



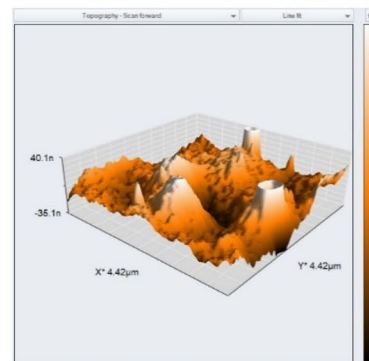
M4



M5



M6



M7

Table 3 Surface roughness parameters of the prepared membranes

Membrane samples	S_a (nm)	S_q (nm)	S_y (nm)
M1	18.61	22.94	159.59
M2	13.55	16.80	115.13
M3	8.74	9.14	13.78
M4	9.73	11.46	50.06
M5	2.99	3.69	13.78
M6	6.17	7.32	16.83
M7	9.07	10.70	37.97

Results and discussion

Characterization of the functionalized mesoporous

The characterization results of KIT-6 and H-KIT-6 are presented in Figs. 1a–h. Figures 1a, b represent FT-IR spectra for KIT-6 and H-KIT-6, respectively. The vibration bands at ~ 1087 and 463 cm^{-1} were assigned to the stretching and bending modes of siloxane groups (Si–O–Si), respectively. Silanol groups (Si–OH) were detected by the broad peak at $\sim 3424\text{ cm}^{-1}$ (stretching band) and a weak peak at 965 cm^{-1} (bending band). The peak at a wavenumber of 3437 cm^{-1} attributed to the hydroxyl and amine groups (Aslam et al. 2016). Besides, the modification of KIT-6 by H-acids was proved by the bands at 1115 and 1271 cm^{-1} , corresponding to the stretching vibration of C–S, C–N, C–O and aromatic rings, respectively. The bands of S–H (2899 cm^{-1}), CH_2 (2960 cm^{-1}), N–H (1723 cm^{-1}), S=O (1462 and 1388 cm^{-1}) were appeared for H-KIT-6, while they were disappeared for KIT-6, indicating an appropriate insertion of H-acids onto KIT-6. The intensity of the

stretching band of OH (around 3437 cm^{-1}) for H-KIT-6 was higher than KIT-6 representing an improved hydrophilicity for H-KIT-6 rather than KIT-6 (Zarabadi-Poor et al. 2013).

Moreover, XRD patterns of KIT-6 and H-KIT-6 mesoporous are shown in Fig. 1c. As can be seen, the broad characteristic peak at $15\text{--}35^\circ$ was related to the mesoporous constituents (Gopinath et al. 2018; Police et al. 2015). The peaks observed at 18.62 , 22.37 , 31.37 and 42.12° corresponded to the H-Acid (Neofotistou et al. 2007). Moreover, zeta potential was utilized to assess the surface charge of KIT-6 and H-KIT-6 as reported in Fig. 1d, f, respectively. From Fig. 1d, e, -38.7 mV versus -6.42 mV was reported for H-KIT-6 compared to KIT-6, indicating an enhanced negative charge of the surface of H-KIT-6 rather than KIT-6. Also, FESEM images of KIT-6 and H-KIT-6 are illustrated in Fig. 1e and h, respectively. As could be observed in figures, the surface of H-KIT-6 was harsher compared to KIT-6 and also the rock-like amorphous morphology of H-KIT-6 is highlighted.

Characterization of the fabricated membranes

FESEM images of the cross-sectional morphologies for all the fabricated membranes are shown in Fig. 2. An asymmetric structure containing a compressed top layer and a porous sublayer for all the fabricate membranes could be observed. Figure 2 shows that the porosity and pore size in the finger-like porous sub-layer were influenced by the loading of additives, so that the bigger macro-voids were obtained by the presence of mesoporous additives. As bigger macro-voids caused higher porosity, the porosity of the fabricated membranes was measured and the achieved data are presented in Table 2. From Table 2, the porosity of the

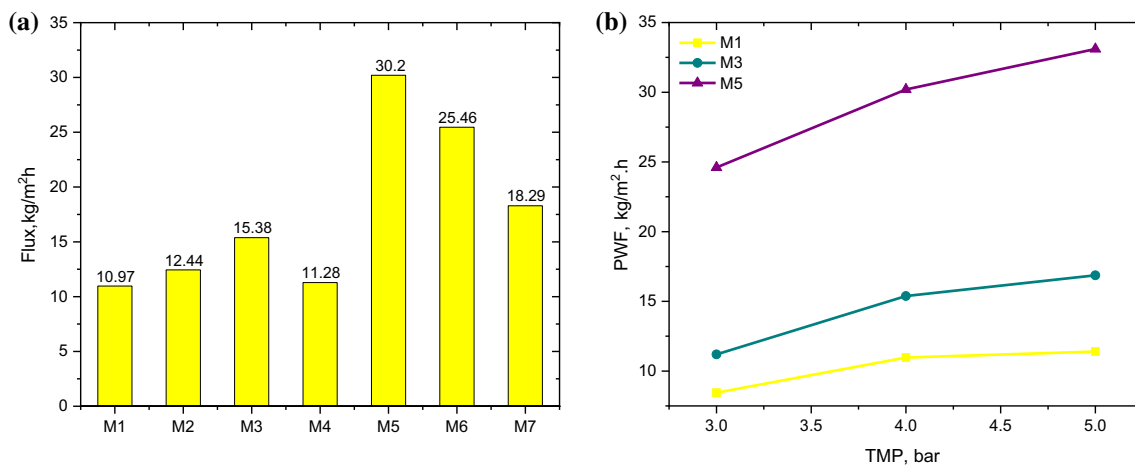


Fig. 5 Pure water flux of all the fabricated membranes at the pressure of 4 bar (a) and the pure water flux of M1, M3 and M5 at different operating pressures (b)

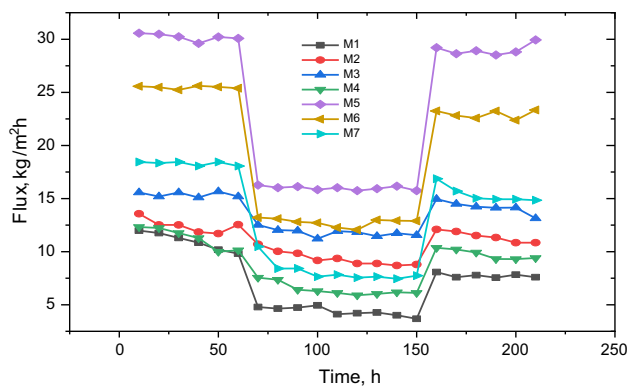


Fig. 6 Permeation flux versus time of the composite mixed matrix membranes

modified membranes was higher than the bare one (M1). Moreover, the highest porosity data were reported as 84% for M5 with 0.1 wt.% of H-KIT-6. However, more increasing H-KIT-6 loading from 0.1 (M5) to 0.5 wt.% (M6) decreased the porosity from 84.7 to 79.8% in which this trend of the porosity data is in a good agreement with FESEM images. As an explanation, the presence of H-KIT-6 with 0.1 wt.% caused an improvement in hydrophilicity of the membrane, thereby mass transfer rate between two phases (solvent and non-solvent) was increased leading to larger pore size and higher porosity. Whereas increasing H-KIT-6 from 0.1 to 0.5 wt.% caused an increase in the viscosity of the solution, resulting a decrease in the mass exchange rate, smaller pores and lower porosity (Asadi et al. 2022a, b; Vatanpour et al. 2020).

Porosity, water contact angle, average pore size and MWCO of all the synthesized membranes are presented in Table 2. In overall, 0.1 wt.% of H-KIT-6 (M5) showed the

highest porosity (84.7%) and average pore size (0.07 nm). MWCO for each membrane was determined using the PEG rejection data at different molecular weights of PEG. MWCO for the modified membranes was lower than the bare membrane (M1), while the membranes embedded with H-KIT-6 illustrated lower values of MWCO which is in a good agreement with mean pore size data. Lower pore size and MWCO is a sign of higher rejection potential for the membranes embedded with H-KIT-6.

Further, to investigate the hydrophilicity of the fabricated membranes, water contact angles were measured for all the synthesized membranes. From Table 2, it is obvious that the insertion of mesoporous additives decreased water contact angle of the bare membrane (M1). The lowest water contact angles were reported as 46.2° and 37.9° for M3 and M5, respectively. As a result, M5 with 0.1 wt.% of H-KIT-6 represented the lowest contact angle, the highest hydrophilicity and negative surface charge influenced by more hydrophilic groups like -OH, -NH and -SO₃ on the membrane surface.

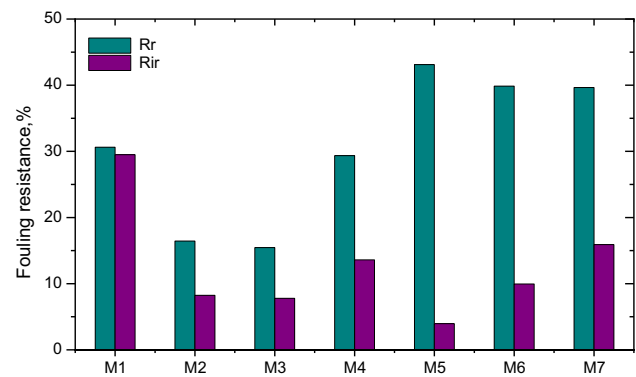


Fig. 8 Fouling resistance of the fabricated membranes

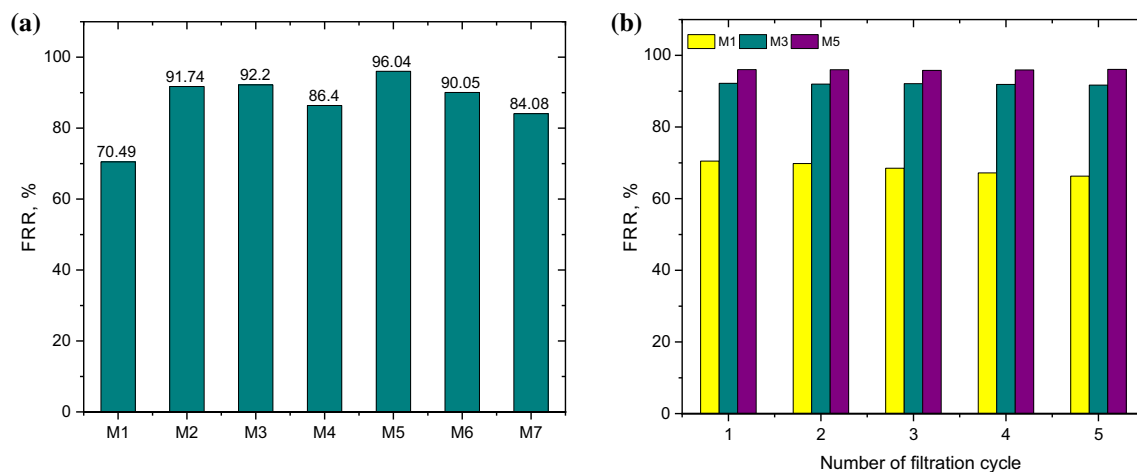


Fig. 7 FRR data of all the fabricated membrane (a) and FRR of M1, M3 and M5 during five repeated filtration cycles of milk solution/deionized water (b)

As a notice, water contact angles were increased slightly at higher loading of KIT-6 and H-MKIT-6 which it may be related to take place agglomeration at high amounts of the additives.

As solute rejection rate is a key factor in the membrane performance and it is influenced by the surface charge in NF filtration membranes significantly, zeta potential of M3 and M5 (which showed the lowest contact angle) was measured and compared with the bare membrane (M1) at different pHs (Fig. 3). The surface negative charge of the bare membrane was enhanced by adding additives as shown in Fig. 3. However, M5 (embedded with H-MKIT-6) represented higher values of negative surface charges compared to M3 (embedded with KIT-6) at all three levels of pH resulted from the presence of hydrophilic functional groups ($-\text{OH}$, $-\text{NH}$ and $-\text{SO}_3$) on the membrane surface. More negative surface charge obtained for M5 is compromised by its lower contact angle (37.9°) which these features tailor membranes to present better performance in the terms of antifouling feature and permeate flux (Jin et al. 2021; Moradi et al. 2021; Mu et al. 2020).

Moreover, the roughness of all the fabricated membranes was evaluated by AFM as illustrated in Fig. 4. It should be noticed that the peaks and valleys on the surface were recognized by the brightest and darkest regions and the roughness parameters of the synthesized membranes are presented in Table 3. Average roughness, root mean square of Z data and the distance between the highest peak and the lowest valley were reported as S_a , S_q and S_y , respectively. From Fig. 4, the surface of M3 and M5 represented more flat surface with respect to the others and the roughness of the bare membrane surface (M1) was decreased by insertion 0.5 wt% of KIT-6 (M3) and 0.1 wt.% of H-KIT-6 (M5). Likewise, the data reported in Table 3 were in good agreement with the AFM figures, so that the maximum and minimum S_a were 18.61 and 2.99 nm for M1 and M5, respectively. Also, from Table 3,

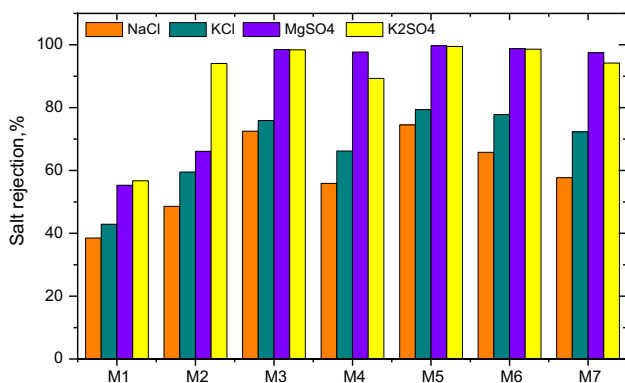


Fig. 9 Salt rejection of the all fabricated membranes (feed concentration of 200 mg/l for salts)

Sa data showed an increasing trend from 2.99 to 9.07 nm with increasing loading rate of H-KIT-6 from 0.1 to 1 wt.% (corresponding to M5 and M7) as a consequence of agglomeration phenomenon at high loading of the additive (Gholami et al. 2021).

Assessment of pure water flux

Pure water fluxes of all the fabricated membranes were measured under the pressure of 4 bar and presented in Fig. 5a. From the figure, pure water flux of the bare membrane was improved with adding KIT-6 and H-KIT-6, though the effect of H-KIT-6 on the response was more significant. As an explanation, the membranes embedded with H-KIT-6 were more hydrophilic as a result of more hydrophilic groups on their surfaces as discussed earlier which led to enhanced pure water flux (see water contact angle, Table 2). Furthermore, the maximum pure water flux was reported as $30.2 \text{ kg/m}^2 \text{ h}$ for M5 with 0.1 wt.% of H-KIT-6. As a notice, with increasing the loading of H-KIT-6 to 1.0 wt.% (M7), pure water flux decreased to $18.29 \text{ kg/m}^2 \text{ h}$. This observed trend for pure water flux is compromised by the results of porosity and water contact angle presented in Table 2. From Table 2, with increasing loading of H-KIT-6 from 0.1 to 1.0 wt.%, porosity was decreased from 84.7 to 63.8% and also water contact angle was increased from 37° to 45° resulted in a decreasing trend in pure water flux. Likewise, M3 with 0.5 wt.% of KIT-6 loading showed the highest pure water flux among the membranes embedded with KIT-6 (M2, M3 and M4). Therefore, M3 and M5 were the optimum membranes for the series of KIT-6- and H-KIT-6-modified membranes. To assess the effect of operating pressure on the pure water flux, M1, M3 and M5 were operated under operating pressures range of 3–5 bar and the measured data are presented in Fig. 5b. According to the figure, M5 was more influenced by increasing the operating pressure compared to M3 and M1 resulted from its higher porosity. In overall, pure water flux was increased linearly for all of the tested membranes with increasing the operating pressure (Oskoui et al. 2019; Vatanpour et al. 2020).

Assessment of antifouling performance

Antifouling properties of the fabricated membranes were evaluated by filtration milk solution (1000 ppm) as a foulant agent under the operating pressure of 4 bar. In this mean, three steps were performed including filtration of distilled water, milk solution and distilled water in sequence. From Fig. 6, the permeate flux was decreased significantly for all the membranes when milk solution was passed through the dead-end setup as a result of fouling phenomena on the

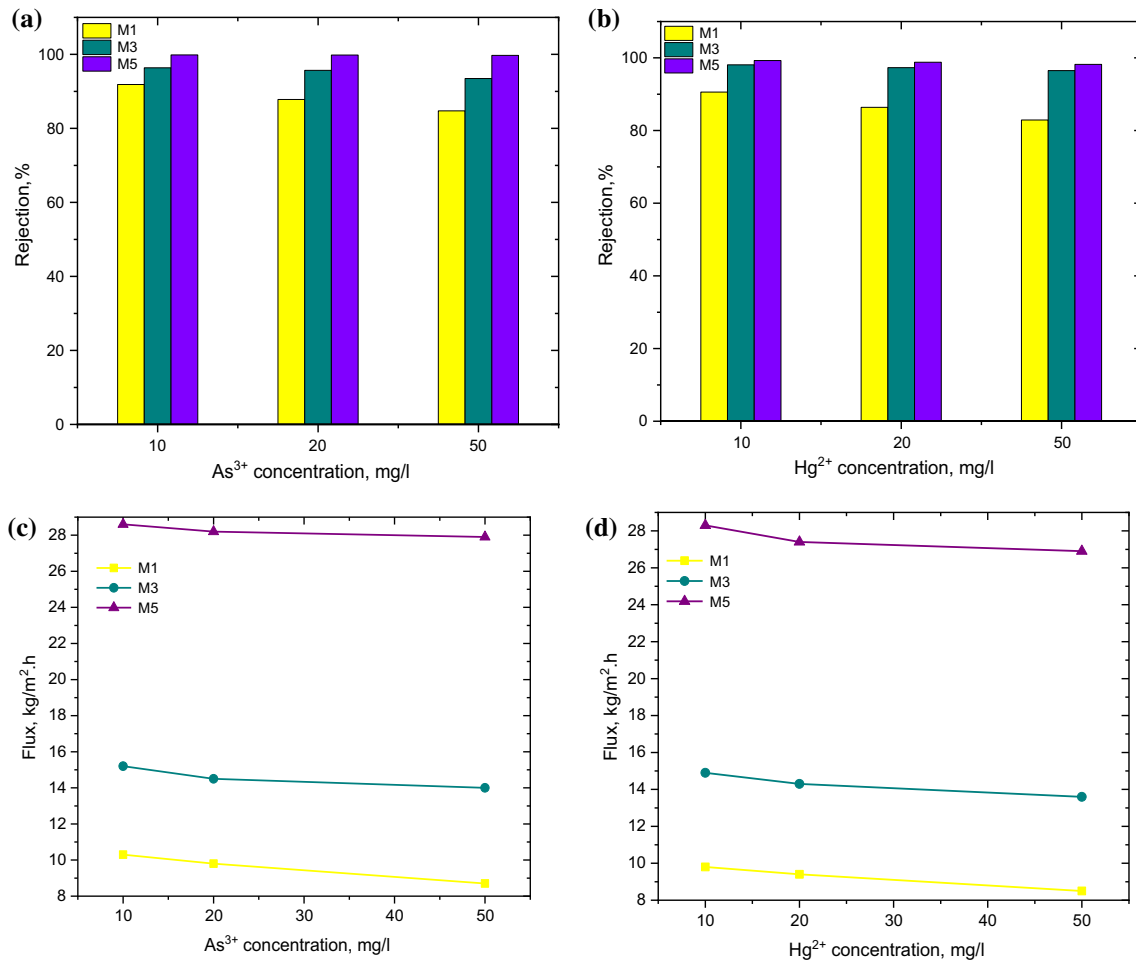


Fig. 10 The rejection data of As³⁺ (a), Hg²⁺ (b) and permeation flux data of As³⁺ (c) and Hg²⁺ (d) for M1, M3 and M5 membranes at different feed concentrations of 10, 20 and 50 mg/l

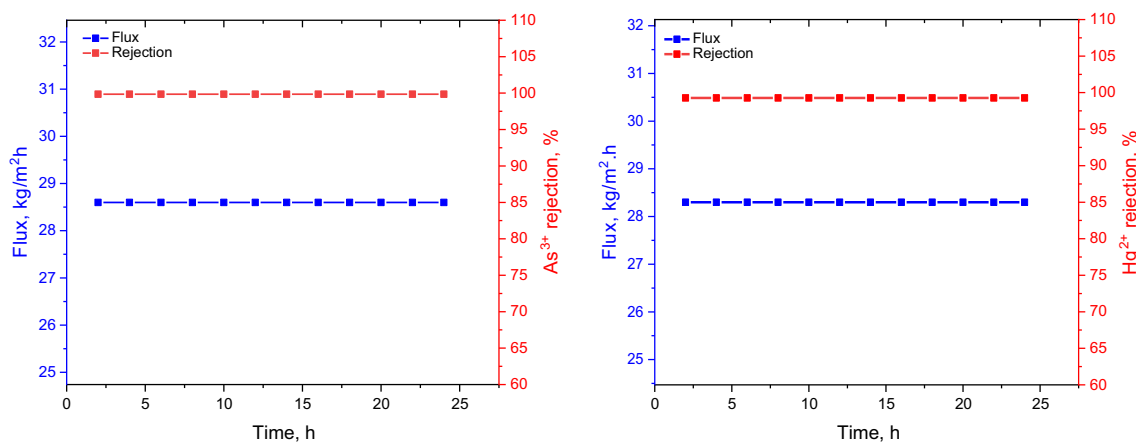


Fig. 11 The rejection and permeation flux of M5 versus time for a As³⁺ and b Hg²⁺

Table 4 The ion concentrations and total hardness of Gachsaran brackish water before and after filtration by the optimum membrane (M5)

	SO ₄ ²⁻ (mg/l)	Ca ²⁺ (mg/l)	Mg ²⁺ (mg/l)	Total hardness (mg CaCO ₃ /l)
Before separation	29.1	582	28	610
After separation	1.1	17.46	0.84	18.3

Table 5 Performance of M5 and a commercial membrane in the same operating condition

	M5	Commercial
Pure water flux, kg/m ² h	30.2	14.9
MgSO ₄ rejection, %	99.7	76.5

The operation condition: 200 ppm MgSO₄, dead-end setup, 4 bar

membrane surface. Nevertheless, the modified membranes showed higher values of permeate flux for all three steps rather than M1, verifying the positive effects of both additives on the bare membranes. Similar to pure water flux data, the membranes embedded with H-KIT-6 (M5, M6 and M7) represented supreme permeate flux rather than the others. The maximum permeate flux for all three steps was reported for M5 with 0.1 wt.% of H-KIT-6. Generally, H-KIT-6 is recognized as an effective additive in terms of increasing hydrophilicity, porosity, permeate flux and antifouling features (Farahani & Vatanpour, 2018; Mohammadnezhad et al. 2019).

Sidelong permeate flux, flux recovery ration (FRR) is another important parameter to investigate antifouling features of the fabricated membranes. Therefore, in the present study FRR was calculated for each membrane as shown in Fig. 7 a. Based on the FRR data, the presence of KIT-6 and H-KIT-6 improved FRR value and antifouling properties, however H-KIT-6 with 0.1 wt.% of loading showed the better performance and higher FRR value. FRR was enhanced from 70.49% for M1 (the bare membrane) to 96.04% for M5 (0.1 wt.% of H-KIT-6). This result could be explained by the inherent hydrophilicity of H-KIT-6 which forms H₂O layer on the membrane surface and prevents adhesion of foulant agent to the membrane surface. In overall, M3 and M5 presented higher values of FRR for series modified membranes with KIT-6 and H-KIT-6, respectively, similar to pure water flux data. Also, FRR values of M3 and M5 as representative of both series of the modified membranes were measured for five sequential filtration cycles of milk solution/deionized water to evaluate the repeatability of the reported FRR

values (Fig. 7b). The achieved results verified the stable and enhanced antifouling properties of M5 over five sequential cycle compared to M3 and M1 (Mohammadnezhad et al. 2019; Safarpour et al. 2016).

To present more deep assessment on antifouling properties, irreversible, reversible and total fouling resistances (*R_{ir}*, *R_r* and *R_t*) of all the fabricated membranes were calculated as presented in Fig. 8. As a fact, reversible fouling could be eliminated by washing as this kind of fouling is temporary. Despite of reversible, irreversible fouling is permanent fouling resulted from pore blocking which could be removed via chemical methods. As observed from Fig. 7, M2–M7 showed lower values of *R_{ir}* compared to M1 and the relatively equal *R_r* and *R_t* was reported for M1 (higher than 29%). As a result, the application of H-KIT-6 in the mixed matrix of membrane decreased *R_{ir}* expressively, so that the lowest value of *R_{ir}* (3.96%) was achieved for M5 with 0.1 wt.% of H-KIT-6 due to its enhanced hydrophilicity and smoothness of the membrane surface. As an outcome, M5 could act as a decent NF membrane in terms of permeate flux and antifouling properties (Safarpour et al. 2016).

Salt rejection

The rejection performance of all the synthesized membranes was evaluated by rejecting four different salts including K₂SO₄, MgSO₄, KCl and NaCl in which the achieved data are presented in Fig. 9. The salt concentration and pH of each salt solution was 0.2 g/L and 6. From Fig. 9, salt rejection followed the order of MgSO₄ > K₂SO₄ > KCl > NaCl compromised by the rejection trend of negatively charged NF membranes. It should be mentioned that the negatively charged surface of NF membrane repulse SO₄²⁻ as divalent anion is more significant compared to Cl⁻ based on Donnan effect. Thus, the rejection data of MgSO₄ and K₂SO₄ were higher than KCl and NaCl. Along with Donnan effect, the hydrated radius of Cl⁻ and SO₄²⁻ are 3.32 and 3.79 Å, respectively, resulted in more rejection of SO₄²⁻ compared to Cl⁻. Also, the hydration radius of Mg²⁺ (0.43 nm) was greater than K⁺ and Na⁺ (0.33 and 0.36 nm) and also Mg²⁺ has higher charge density as a divalent cation, resulting a higher attraction between negative surface of membrane and Mg²⁺ which finally led to higher rejection of Mg²⁺. Similar to pure water flux and FRR data, salt rejection efficiency was improved with embedding KIT-6 and H-KIT into the mixed matrix membrane. The lowest salt rejection was reported for M1 (the bare membrane) and the highest salt rejection was obtained for M5 (0.1 wt.% of H-KIT-6) for all different salts. Likewise, M3 (0.5 wt.% of KIT-6) represented the highest salt rejection for all four salts in the series of membranes embedded with KIT-6. These results were in a good agreement with zeta potential data of M5, M3 and M1 presented in Fig. 3. As reported in Fig. 3, zeta potential data followed

Table 6 The heavy metals/salts rejection data of some nanofiltration membranes

Membrane	Techniques	PWF, kg/m ² .h	Heavy metal /salt	Rejection, %	Refs.
TFN-UiO-66-NH ₂	TFN	12	MgSO ₄	92	(Liu et al. 2020)
CNC-TFC	TFC	16.45	NaCl	22.7	(Bai et al. 2018)
			MgSO ₄	98.8	
Sulfaguanidine TFC	TFC	–	NaCl	36.7	(Zhang et al. 2019)
			MgSO ₄	94.5	
PS/PES TFC	TFC	11.9	NaCl	39.8	(Wei et al. 2013)
			MgSO ₄	96.2	
TFN-mBTO-E	TFC	5.8	As	97	(Pu et al. 2021)
PA-CSBF	TFC	–	As	98	(Zeeshan et al. 2020)
PAA-PVDF 700	TFC	–	Hg	97	(Islam et al. 2020)
GO-PES	TFC	26.3	Hg	80.3	(Chen et al. 2019)
NF-SS/NF-SH	TFC	–	Hg	99.8	(Zhang et al. 2020)
			NaCl	45.2	
			MgSO ₄	96.7	
MoS ₂ -PSBMA/PES	MMM	18.5	Na ₂ SO ₄	2.2	(Liang et al. 2019)
			MgSO ₄	0.3	
ZIF-8/(TA-Zn ²⁺) ₂ /PES	MMM	5.1	NaCl	55.2	(Xiao et al. 2021)
			MgSO ₄	85.9	
PVDF/SMA/CNTCOOH	MMM	–	NaCl	1.7	(Kang et al. 2021)
			MgSO ₄	1.2	
PSf/GO-vanillin	MMM	35	NaCl	25.4	(Yadav et al. 2022)
			MgSO ₄	92.5	
PMIA	MMM	–	As	90	(Zhao et al. 2012)
PPSU/MWCNTs	MMM	–	Hg	76	(Chandrashekar et al. 2019)
N30F	Commercial	–	As	78	(Figoli et al. 2010)
NF90			As	94	
PSf/H-KIT-6	MMM	30.2	As	99.85	This work
			Hg	99.27	
			NaCl	74.5	
			MgSO₄	99.7	

The obtained results of the current work were specified with bold for getting readers' attention

the order of M5 > M3 > M1 for the range of pH between 4 and 10 (Nightingale Jr, 1959; Wang et al. 2016).

Rejection of heavy metal ions

As the existence of heavy metals in water resources is a serious threat for human health, in the present study, the performance of the optimum membranes including M3 (for the series of membranes embedded with KIT-6) and M5 (for the modified membranes with H-KIT-6) to reject two different heavy metal ions (Hg²⁺ and As³⁺) has been compared with M1 (the bare membrane).

In this mean, the rejection and permeation flux of the mentioned membranes (M1, M3 and M5) at concentration of 10, 20 and 50 mg/l of Hg²⁺ and As³⁺ were measured and reported in Fig. 10a–d. As observed from Fig. 10a, b, the rejections of Hg²⁺ and As³⁺ for M1 were decreased obviously by increasing the convention of ions from 10 to 50 mg/l. Likewise, M3 presented a gentle reduction for rejecting of Hg²⁺ and As³⁺ with increasing the concentration

of ions, while M5 showed a nearly constant rejection data at different concentrations of heavy metal ions and decreasing trend was not significant, indicating the high potential of M5 for the rejection of heavy metals. Generally, in spite of smaller hydrated radius of As³⁺ (0.35 nm) compared to Hg²⁺ (0.422 nm), the rejection of As³⁺ was higher than that Hg²⁺ for all the three tested membranes. This result could be explained by the high charge density of As³⁺ led to more effective adsorption on the negatively charged membrane surface. From Figs. 10 a and b, M5 presented the highest rejection performance for both heavy metal ions, so that the rejection data of M5 were 99.735% and 98.2% for As³⁺ and Hg²⁺ with 50 mg/l of concentration. Furthermore, the rejection flux data of As³⁺ and Hg²⁺ are reported in Fig. 10c, d. According to the figures, the permeate flux of M5 was significantly higher than M3 and M1 at different concentrations of heavy metal ions as a result of higher hydrophilic property of M5 verified by lower reported water contact angle (see Table 2). Permeate flux data of M5 were in the range of 27–28.6 kg/m².h for As³⁺ and Hg²⁺ rejection with

concentration of 10–50 mg/l. It should be noticed that the membrane performance in rejecting heavy metal ions and permeate flux followed the order of M5 > M3 > M1. The steady and higher rejection of M5 is related to the higher negatively charge of the membrane surface caused higher interaction between surface membrane and heavy metals ions (Bandehali et al. 2020; Nightingale 1959; Shukla et al. 2018).

In the next step, in order to present more deep assessment on the ability of M5 to reject heavy metals, a long-term study to remove both studied heavy metals with concentration of 10 mg/l and operating pressure of 4 bar was carried out. The obtained data over 24 h are displayed in Fig. 11a, b. As illustrated in the figures, the rejection and permeate flux of As³⁺ and Hg²⁺ were constant over 24 h, indicating a supreme and stable performance of M5 for heavy metal rejection resulted from a decent permanency of H-KIT-6 in the mixed matrix membrane.

Gachsaran brackish water filtration

Gachsaran brackish water was passed through M5 membrane to evaluate its performance for rejecting different salts from a real case brackish water which is multipollutant solution. Table 4 presented the concentrations of SO₄²⁻, Ca²⁺ and Mg²⁺ and also total hardness before and after filtration by M5. From Table 4, M5 presented an outstanding performance to remove ions from a real case as total hardness was decreased from 610 to 18.3 mg/l. Besides, around 565 mg/l, 28 mg/l and 27 mg/l of Ca²⁺, SO₄²⁻ and Mg²⁺ were rejected, respectively. As a conclusion, H-KIT-6 with 0.1 wt.% tailor PSf nanofiltration membrane to reject different salts and ions from multipollutant solution and real cases of brackish water.

A comparative performance with commercial membrane

The performance of M5 (optimal membrane modified with H-KIT-6) and a commercial membrane (WMC110 dNF80) was compared to reject MgSO₄ in the same operating conditions (as presented in Table 5). The comparable data are summarized in Table 5. From the table, an enhanced pure water flux could be observed for M5 rather than the used commercial nanofiltration membrane. Besides, the rejection of MgSO₄ was found to be 99.7 and 76.5% for M5 and the commercial membrane, respectively. It is clearly found that H-KIT-6 plays an important role to improve the performance of nanofiltration membrane in terms of PWF and salt rejection.

A comparative review on nanofiltration membranes

To compare the performance of M5 (the optimum membrane) with the literature, the rejection data of heavy metals/salts for some nanofiltration membranes prepared with different modification techniques are illustrated in Table 6. From the table, it could be observed that the rejection data of NaCl/MgSO₄ for the reported membranes were lower than the data obtained in the current study. NaCl rejection was in the range of 22.7–55.2%, while 74% of NaCl was rejected in the current study (M5). However, MgSO₄ rejection approximately was the same range for the membrane modified with TFN- UiO-66-NH₂ and PSf/H-KIT-6 (M5: current study), PWF of M5 was 30.2 kg/m².h compared with 12 kg/m².h for TFN- UiO-66-NH₂.

Besides, M5 showed higher performance for rejecting heavy metals compared to the other studies, so that more than 99% of rejection data was found for both As and Hg. The polarized ferroelectric membrane (TFN-mBTO-E) shows 97% of As rejection, whereas its pure water flux was low rather than the membrane embedded with PSf/H-KIT-6 (5.8 kg/m² h versus 30.2 kg/m² h), verifying the efficient amended procedure in the present study. Also, TFC membrane modified with graphene oxide (GO) represented 80.3% of Hg rejection with pure water flux of 26.3 kg/m² h, corroborating that PSf/H-KIT-6 is more prone to reject heavy metals with high pure water flux. To sum up, the detrimental impact of TFC on the pure water flux was clearly observed in the mentioned researches, while PSf/H-KIT-6 presents high water flux aside from high rejection rate of salts.

Moreover, some studies with mixed matrix membrane are presented in Table 6. From the table, the maximum pure water flux was reported for PSf/GO-vanillin (35 kg/m² h); however, the rejection of NaCl and MgSO₄ was 25.4% and 92.5%, respectively (versus 74.5% and 99.7% for the present study). Therefore, it could be concluded that PSf/H-KIT-6 was outperformed in comparison with the researches utilized by both TFC and mixed matrix methods. As a result, the comparative data of PSf/H-KIT-6 and the nanofiltration membranes reported in the literature illustrated the outstanding performance of M5 (PSf/H-KIT-6) in terms of rejection and PWF which makes it a decent proposal for efficient and economic brackish water treatment.

Thin-film composite (TFC), mixed matrix membrane (MMM), thin-film nanocomposite (TFN), Cellulose nanocrystals (CNCs), polysulfone (PS), polyethersulfone (PES), polarized ferroelectric membrane (mBTO-E), core shell biofunctionalized (CSBF), polyacrylic acid (PAA), polyvinylidene fluoride (PVDF), graphene oxide (GO), 2-methacryloyloxy ethyl dimethyl (3-sulfopropyl)-ammonium hydroxide sulfobetaine methacrylate (MoS 2 -PSBMA), styrene-maleic anhydride (SMA), carboxylated carbon

nanotubes (CNT-COOH), poly(m-phenylene isophthalamide) (PMIA), polyphenylsulfone (PPSU).

Conclusions

In the present research, KIT-6 was modified by H-acid and the effect of both KIT-6 and H-KIT-6 additives on the nanofiltration membrane performance for rejecting heavy metal ions and different salts was evaluated. According to the characterization and performance tests, H-KIT-6 with 0.1 wt.% not only reduced water contact angle and the surface roughness, but also increased negative surface charge, porosity, pure water flux, heavy metal ions rejection and antifouling properties. As a result, the well-performed membrane (0.1 wt.% of H-KIT-6) rejected 99.27% and 99.85% of Hg^{2+} and As^{3+} , respectively, for a long time operation over 24 h with constant permeate flux (over $28 \text{ kg/m}^2\cdot\text{h}$). Likewise, the highest salt rejection was obtained for membrane embedded with 0.1 wt.% of H-KIT-6 with the order of $\text{MgSO}_4 > \text{K}_2\text{SO}_4 > \text{KCl} > \text{NaCl}$. Finally, the performance of the optimum membrane was investigated to reject salts from a real case brackish water in which total hardness of the mentioned water was reduced from 610 to $18.3 \text{ mg CaCO}_3/\text{l}$. As a conclusion, H-KIT-6 mesoporous was used efficaciously to improve the performance and features of nanofiltration membrane with mixed matrix of PSf polymer.

Funding The authors declare that they have no known competing financial interests or personal relationships that could have appeared to influence the work reported in this paper.

Declarations

Conflict of interest On behalf of all authors, the corresponding author states that there is no conflict of interest.

Open Access This article is licensed under a Creative Commons Attribution 4.0 International License, which permits use, sharing, adaptation, distribution and reproduction in any medium or format, as long as you give appropriate credit to the original author(s) and the source, provide a link to the Creative Commons licence, and indicate if changes were made. The images or other third party material in this article are included in the article's Creative Commons licence, unless indicated otherwise in a credit line to the material. If material is not included in the article's Creative Commons licence and your intended use is not permitted by statutory regulation or exceeds the permitted use, you will need to obtain permission directly from the copyright holder. To view a copy of this licence, visit <http://creativecommons.org/licenses/by/4.0/>.

References

- Abbasi Eskandary N, Pakizeh M, Namvar-Mahboub M (2021) Nanomodification of the polyvinyl alcohol/organic acid-modified polyvinylidene fluoride thin-film composite membrane and its application in the nanofiltration process. *Macromol Mater Eng* 306(5):2000767
- Asadi A, Gholami F, Zinatizadeh A, Jaberi H (2022a) Application of novel nanofiltration membranes embedded with mesoporous carbon based nanoparticles for desalination and dye removal. *Chem Pap* 76(3):1349–1363
- Asadi A, Gholami F, Zinatizadeh AA (2022b) Enhanced oil removal from a real polymer production plant by cellulose nanocrystals-Serine incorporated polyethersulfone ultrafiltration membrane. *Environ Sci Pollut Res*. <https://doi.org/10.1007/s11356-021-18055-4>
- Aslam S, Subhan F, Yan Z, Peng P, Qiao K, Xing W, Zeng J (2016) Facile fabrication of Ni-based KIT-6 for adsorptive desulfurization. *Chem Eng J* 302:239–248
- Bai L, Liu Y, Bossa N, Ding A, Ren N, Li G, Wiesner MR (2018) Incorporation of cellulose nanocrystals (CNCs) into the polyamide layer of thin-film composite (TFC) nanofiltration membranes for enhanced separation performance and antifouling properties. *Environ Sci Technol* 52(19):11178–11187
- Bandehali S, Moghadassi A, Parvizian F, Zhang Y, Hosseini SM, Shen J (2020) New mixed matrix PEI nanofiltration membrane decorated by glycidyl-POSS functionalized graphene oxide nanoplates with enhanced separation and antifouling behaviour: heavy metal ions removal. *Sep Purif Technol* 242:116745
- Chandrashekar N, Isloor A, Lakshmi B, Marwani H, Khan I (2019) Polyphenylsulfone/multiwalled carbon nanotubes mixed ultrafiltration membranes: fabrication, characterization and removal of heavy metals Pb^{2+} , Hg^{2+} , and Cd^{2+} from aqueous solutions. *Arab J Chem*. <https://doi.org/10.1016/j.arabj.2019.10.007>
- Chen H, Wu H, Wang Q, Ji L, Zhang T, Yang H (2019) Separation performance of Hg^{2+} in desulfurization wastewater by the graphene oxide polyethersulfone membrane. *Energy Fuels* 33(9):9241–9248
- Chitpong N, Husson SM (2017) Polyacid functionalized cellulose nanofiber membranes for removal of heavy metals from impaired waters. *J Membr Sci* 523:418–429
- Farahani MHDA, Vatanpour V (2018) A comprehensive study on the performance and antifouling enhancement of the PVDF mixed matrix membranes by embedding different nanoparticles: clay, functionalized carbon nanotube, SiO_2 and TiO_2 . *Sep Purif Technol* 197:372–381
- Figoli A, Cassano A, Criscuoli A, Mozumder MSI, Uddin MT, Islam MA, Drioli E (2010) Influence of operating parameters on the arsenic removal by nanofiltration. *Water Res* 44(1):97–104
- Gao J, Wang KY, Chung T-S (2020) Design of nanofiltration (NF) hollow fiber membranes made from functionalized bore fluids containing polyethyleneimine (PEI) for heavy metal removal. *J Membr Sci* 603:118022
- Gholami F, Zinatizadeh S, Kamrani SN, Zinatizadeh AA, Bahrami K (2021) Color removal from wastewater using a synthetic high-performance antifouling GO-CPTMS@ Pd-TKHPP/polyether sulfone nanofiltration membrane. *Environ Sci Pollut Res*: 1–16.
- Giagnorio M, Steffenino S, Meucci L, Zanetti MC, Tiraferri A (2018) Design and performance of a nanofiltration plant for the removal of chromium aimed at the production of safe potable water. *J Environ Chem Eng* 6(4):4467–4475
- Gnanasekaran G, Arthanareeswaran G, Mok YS (2021) A high-flux metal-organic framework membrane (PSF/MIL-100 (Fe)) for the removal of microplastics adsorbing dye contaminants from textile wastewater. *Sep Purif Technol* 277:119655
- Gopinath S, Kumar PV, Kumar PSM, Arafath KY, Sivanesan S, Baskaralingam P (2018) Cs-tungstosilicic acid/Zr-KIT-6 for esterification of oleic acid and transesterification of non-edible oils for green diesel production. *Fuel* 234:824–835
- Ikehata K, Zhao Y, Kulkarni HV, Li Y, Snyder SA, Ishida KP, Anderson MA (2018) Water recovery from advanced water purification

- facility reverse osmosis concentrate by photobiological treatment followed by secondary reverse osmosis. *Environ Sci Technol* 52(15):8588–8595
- Islam MS, Vogler RJ, Abdullah Al Hasnine SM, Hernández S, Malekzadeh N, Hoelen TP, Bhattacharyya D (2020) Mercury removal from wastewater using cysteamine functionalized membranes. *ACS omega* 5(35):22255–22267
- Jin P, Zhu J, Yuan S, Zhang G, Volodine A, Tian M, Van der Bruggen B (2021) Erythritol-based polyester loose nanofiltration membrane with fast water transport for efficient dye/salt separation. *Chem Eng J* 406:126796
- Kamari S, Shahbazi A (2020) Biocompatible $\text{Fe}_3\text{O}_4@ \text{SiO}_2\text{-NH}_2$ nanocomposite as a green nanofiller embedded in PES–nanofiltration membrane matrix for salts, heavy metal ion and dye removal: long-term operation and reusability tests. *Chemosphere* 243:125282
- Kang D, Shao H, Chen G, Dong X, Qin S (2021) Fabrication of highly permeable PVDF loose nanofiltration composite membranes for the effective separation of dye/salt mixtures. *J Membr Sci* 621:118951
- Kiran SA, Thuyavan YL, Arthanareeswaran G, Matsuura T, Ismail A (2016) Impact of graphene oxide embedded polyethersulfone membranes for the effective treatment of distillery effluent. *Chem Eng J* 286:528–537
- Li H, Mu P, Li J, Wang Q (2021) Inverse desert beetle-like ZIF-8/PAN composite nanofibrous membrane for highly efficient separation of oil-in-water emulsions. *J Mater Chem A* 9(7):4167–4175
- Li N, Wang W, Ma C, Zhu L, Chen X, Zhang B, Zhong C (2022) A novel conductive rGO/ZnO/PSF membrane with superior water flux for electrocatalytic degradation of organic pollutants. *J Membr Sci* 641:119901
- Liang X, Wang P, Wang J, Zhang Y, Wu W, Liu J, Van der Bruggen B (2019) Zwitterionic functionalized MoS₂ nanosheets for a novel composite membrane with effective salt/dye separation performance. *J Membr Sci* 573:270–279
- Liu H, Zhang M, Zhao H, Jiang Y, Liu G, Gao J (2020) Enhanced dispersibility of metal–organic frameworks (MOFs) in the organic phase via surface modification for TFN nanofiltration membrane preparation. *RSC Adv* 10(7):4045–4057
- López J, Reig M, Vecino X, Gibert O, Cortina J (2020) Comparison of acid-resistant ceramic and polymeric nanofiltration membranes for acid mine waters treatment. *Chem Eng J* 382:122786
- Mohammadnezhad F, Feyzi M, Zinadini S (2019) A novel Ce-MOF/PES mixed matrix membrane; synthesis, characterization and antifouling evaluation. *J Ind Eng Chem* 71:99–111
- Moradi G, Zinadini S, Rajabi L, Derakhshan AA (2020) Removal of heavy metal ions using a new high performance nanofiltration membrane modified with curcumin boehmite nanoparticles. *Chem Eng J* 390:124546
- Moradi G, Heydari R, Zinadini S, Rahimi M, Gholami F (2021) High-performance nanofiltration membranes consisting of the new functionalized mesoporous for enhanced antifouling attributes and simultaneous removal of salts, dyes and heavy metals. *Environ Technol Innov*. <https://doi.org/10.1016/j.eti.2021.101929>
- Mu T, Zhang H-Z, Sun J-Y, Xu Z-L (2020) Three-channel capillary nanofiltration membrane with quaternary ammonium incorporated for efficient heavy metals removal. *Sep Purif Technol* 248:117133
- Neofotistou E, Malliakas CD, Trikalitis PN (2007) Novel coordination polymers based on the tetrathioterephthalate dianion as the bridging ligand. *Inorg Chem* 46(21):8487–8489
- Nightingale E Jr (1959) Phenomenological theory of ion solvation. Effective radii of hydrated ions. *J Phys Chem* 63(9):1381–1387
- Oskoui SA, Vatanpour V, Khataee A (2019) Effect of different additives on the physicochemical properties and performance of NLDH/PVDF nanocomposite membrane. *Sep Purif Technol* 209:921–935
- Podgorski J, Berg M (2020) Global threat of arsenic in groundwater. *Science* 368(6493):845–850
- Police AKR, Basavaraju S, Valluri D, Machiraju S (2015) Photocatalytic activity of Ce-modified SBA-15 for the degradation of isoproturon. *Bull Mater Sci* 38(1):227–234
- Pu L, Xu Y, Xia Q, Ding J, Wang Y, Shan C, Pan B (2021) Ferroelectric membrane for water purification with arsenic as model pollutant. *Chem Eng J* 403:126426
- Rahimi Z, Zinatizadeh AA, Zinadini S, van Loosdrecht M, Younesi H (2021) A new anti-fouling polysulphone nanofiltration membrane blended by amine-functionalized MCM-41 for post treating waste stabilization pond's effluent. *J Environ Manage* 290:112649
- Safarpour M, Vatanpour V, Khataee A (2016) Preparation and characterization of graphene oxide/TiO₂ blended PES nanofiltration membrane with improved antifouling and separation performance. *Desalination* 393:65–78
- Samari M, Zinadini S, Zinatizadeh AA, Jafarzadeh M, Gholami F (2020) Designing of a novel polyethersulfone (PES) ultrafiltration (UF) membrane with thermal stability and high fouling resistance using melamine-modified zirconium-based metal-organic framework (UiO-66-NH₂/MOF). *Sep Purif Technol* 251:117010
- Samari M, Zinadini S, Zinatizadeh AA, Jafarzadeh M, Gholami F (2021) A new fouling resistance polyethersulfone ultrafiltration membrane embedded by metformin-modified FSM-16: Fabrication, characterization and performance evaluation in emulsified oil-water separation. *J Environ Chem Eng* 9(4):105386
- Shukla AK, Alam J, Alhoshan M, Dass LA, Ali FAA, Mishra U, Ansari MA (2018) Removal of heavy metal ions using a carboxylated graphene oxide-incorporated polyphenylsulfone nanofiltration membrane. *Environ Sci: Water Res Technol* 4(3):438–448
- Sutton DJ, Tchounwou PB, Ninashvili N, Shen E (2002) Mercury induces cytotoxicity and transcriptionally activates stress genes in human liver carcinoma (HepG2) cells. *Int J Mol Sci* 3(9):965–984
- Vatanpour V, Dehqan A, Harifi-Mood AR (2020) Ethaline deep eutectic solvent as a hydrophilic additive in modification of polyethersulfone membrane for antifouling and separation improvement. *J Membr Sci* 614:118528
- Wang J, Li Y, Zhang Z, Hao Z (2015) Mesoporous KIT-6 silica–polydimethylsiloxane (PDMS) mixed matrix membranes for gas separation. *J Mater Chem A* 3(16):8650–8658
- Wang J, Zhang Y, Zhu J, Hou J, Liu J, Van der Bruggen B (2016) Zwitterionic functionalized layered double hydroxides nanosheets for a novel charged mosaic membrane with high salt permeability. *J Membr Sci* 510:27–37
- Wang Z, Wang Z, Lin S, Jin H, Gao S, Zhu Y, Jin J (2018) Nanoparticle-templated nanofiltration membranes for ultrahigh performance desalination. *Nat Commun* 9(1):1–9
- Wang J, Yu W, Graham NJ, Jiang L (2020) Evaluation of a novel polyamide-polyethylenimine nanofiltration membrane for wastewater treatment: removal of Cu²⁺ ions. *Chem Eng J* 392:123769
- Wei X, Kong X, Sun C, Chen J (2013) Characterization and application of a thin-film composite nanofiltration hollow fiber membrane for dye desalination and concentration. *Chem Eng J* 223:172–182
- Xiao Y, Zhang W, Jiao Y, Xu Y, Lin H (2021) Metal-phenolic network as precursor for fabrication of metal-organic framework (MOF) nanofiltration membrane for efficient desalination. *J Membr Sci* 624:119101
- Yadav S, Ibrar I, Samal AK, Altaee A, Déon S, Zhou J, Ghaffour N (2022) Preparation of fouling resistant and highly perm-selective novel PSf/GO-vanillin nanofiltration membrane for efficient water purification. *J Hazard Mater* 421:126744
- Zarabadi-Poor P, Badiei A, Yousefi AA, Barroso-Flores J (2013) Selective optical sensing of Hg (II) in aqueous media by H-Acid/SBA-15: a combined experimental and theoretical study. *J Phys Chem C* 117(18):9281–9289

- Zeeshan MH, Khan RU, Shafiq M, Sabir A (2020) Polyamide intercalated nanofiltration membrane modified with biofunctionalized core shell composite for efficient removal of arsenic and selenium from wastewater. *J Water Process Eng* 34:101175
- Zeng H, Yu Y, Wang F, Zhang J, Li D (2020) Arsenic (V) removal by granular adsorbents made from water treatment residuals materials and chitosan. *Colloids Surf A* 585:124036
- Zhang H-L, Liu B-H, Yang M, Zhang P, Gai J-G (2019) Sulfaguandine nanofiltration active layer towards anti-adhesive and antimicrobial attributes for desalination and dye removal. *RSC Adv* 9(36):20715–20727
- Zhang H-L, Cai H, Xia Y, Zhang P, Xiong S-W, Gai J-G (2020) An l-cystine/l-cysteine impregnated nanofiltration membrane with the superior performance of an anchoring heavy metal in wastewater. *RSC Adv* 10(6):3438–3449
- Zhao C, Du S, Wang T, Zhang J, Luan Z (2012) Arsenic removal from drinking water by self-made PMIA nanofiltration membrane. *ACES*. <https://doi.org/10.4236/aces.2012.23043>
- Zhao G, Wang X, Li C, Meng H (2020) Superhydrophilic alkynyl carbon composite nanofiltration membrane for water purification. *Appl Surf Sci* 508:144788
- Zhao X, Che Y, Mo Y, Huang W, Wang C (2021) Fabrication of PEI modified GO/MXene composite membrane and its application in removing metal cations from water. *J Membr Sci* 640:119847

Publisher's Note Springer Nature remains neutral with regard to jurisdictional claims in published maps and institutional affiliations.